A fast phosphor imaging diagnostic for two-dimensional plasma fluctuation measurements

A. Liebscher,[a] S. C. Luckhardt, and G. Antar
Center for Energy Research, Fusion Energy Division, Department of Mechanical and Aerospace Engineering, University of California, San Diego, La Jolla, California 92093

S. Zweben
PPPL, Princeton University, Princeton, New Jersey 08543

(Presented on 21 June 2000)

A plasma imaging diagnostic is being developed using a fast time response ZnO:Zn phosphor disk to image plasma density fluctuations in a two-dimensional (2D) region. The plasma sensor consists of an 8.9 cm diameter phosphor coated aluminum disk that is inserted into the plasma and is excited by incident electrons resulting in a cathodoluminescent emission image. The phosphor light distribution is then interpreted as plasma density fluctuations using sheath theory and the phosphor response function. The local luminance S of fluctuating phosphor light is dependent on the incident electron energy E_e and current density through the equation $S(\mathbf{r},t)=e\int R(E_e)(\mathbf{v}\cdot\hat{\mathbf{n}})f_e(\mathbf{r},\mathbf{v},t)d^3v$, where $R(E_e)$ is the energy dependent response function of the phosphor. The phosphor persistence time of 1–10 μs (emulsion dependent) combined with fast intensified charge coupled device camera shutter speeds enables the imaging of plasma fluctuations on microsecond range time scales. Broadband turbulent phosphor light fluctuations ($f\leqslant 500$ kHz) have been measured with photodiode detectors and compared with Langmuir probe data. The 2D phosphor images show density profiles consistent with radial Langmuir probe measurements. Temporal and spatial resolution of the phosphor diagnostic enables 2D imaging of plasma turbulence and coherent modes.
 [DOI: 10.1063/1.1329658]

I. INTRODUCTION

An imaging diagnostic technique has been developed to obtain two-dimensional images of a plasma column ending on a phosphor coated disk. We call this technique the cathodoluminescent phosphor plasma imaging system or CAPPIS. The main advantage of this diagnostic is its ability to image radial and polodial structure of coherent modes and turbulence. The plasma imaging is complementary to diagnostics such as probes that record localized time dependent fluctuations. Recently, the interest in two-dimensional (2D) plasma imaging has increased because of the need to characterize turbulence and intermittent structures in fusion plasmas. Conventional diagnostic methods based on plasma light emission or Langmuir probe arrays usually lack spatial resolution or detect line integrated quantities.[1] Here we present initial results of a high resolution plasma imaging system having local response to plasma density and temperature. In order to confirm the validity of this approach we have compared the time series phosphor light from a point on the phosphor disk to Langmuir probe measurements of fluctuations. Further, we find that the spatial profiles of the electron density determined from the phosphor image agree with Langmuir probe profiles.

II. EXPERIMENTAL SETUP

In our plasma imaging experiments the PISCES–A linear plasma device, Fig. 1, was used to test the response of a ZnO:Zn coated aluminum disk attached to the end of a pneumatically actuated positioning arm. The disk is inserted into the plasma for a short period of time (~1–5 s) in order to reduce heating and erosion of the phosphor coating.[2] The disk is mounted at an angle of 45°, which optimizes the amount of phosphor light received by the fast imaging system and maintains an acceptable field of view. Importantly, the disk diameter (8.9 cm) is larger than the plasma diameter (6 cm) so the entire plasma cross section can be imaged. Phosphor light emitted from the surface of the disk ($\lambda \sim 500$ nm) can be detected using an intensified charge coupled device (CCD) camera or a single channel photodiode detector. The camera has a spatial resolution of $780(h) \times 244(v)$ pixels, and a variable exposure time of 120 ns–16 ms. The camera threshold sensitivity is 3×10^{-7} lm/m^2, and the spectral response of the camera is nearly flat from 450–850 nm and is well suited for imaging the ZnO:Zn phosphor light. In order to remove the background light from the phosphor light we use bandpass optical interference filters centered at $\lambda = 500$ nm with a bandwidth of 60 nm. The digital images are captured from the camera using a high resolution frame capture card and imaging software. The capture system is configured for field mode capture (NTSC, 60 fields/s) in order to avoid overlapping image information. The data obtained from the CAPPIS setup is compared to other plasma diagnostics available on PISCES–A including fast scanning radial and axial Langmuir probes and high bandwidth (10 MHz) photodiode detectors.

[a]Electronic mail: aliebscher@ferp.ucsd.edu

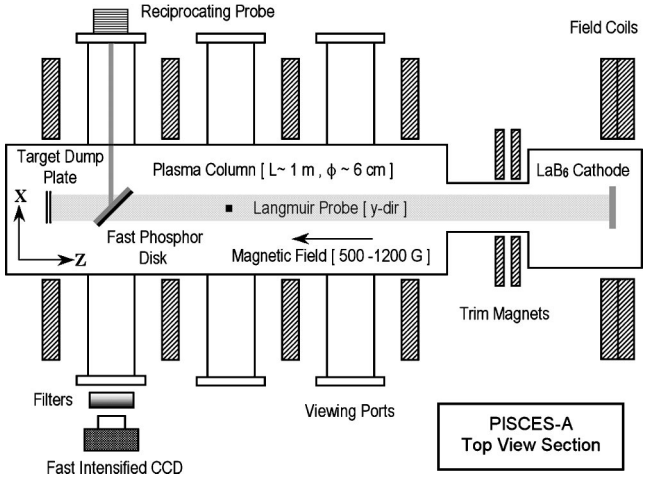

FIG. 1. Diagram of the experimental setup for fast 2D imaging of plasma fluctuations. The CAPPIS phosphor disk is situated within the plasma column at an angle of 45° with respect to the plasma axis providing a view of the phosphor disk through an optical viewport.

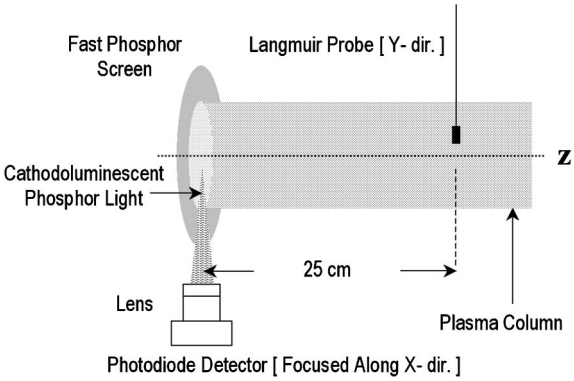

FIG. 2. The photodiode and lens are used to detect local phosphor light fluctuations on the CAPPIS disk, and compared to simultaneously measured plasma density fluctuations obtained with a Langmuir probe. The photodiode lens was focused on a 0.04 cm^2 area, and the Langmuir probe was located upstream.

III. ZnO:Zn IMAGING CHARACTERISTICS

The most important parameters when choosing a phosphor for fast plasma imaging applications are luminous efficiency (η_e), persistence time (τ_p), and threshold electron energy (E_{ec}).[3] The ZnO:Zn phosphor (P24) that we chose has a high luminous efficiency,[4] typically $\eta = 6.8$ lm/W, where η is the luminous flux emitted per unit area divided by the power density of the incident electron beam. It is important to recognize that the luminous efficiency is temperature dependent.[5] We measured the temperature dependence of our ZnO:Zn coating using an ultraviolet source for phosphor excitation and found that the light emission will decrease by ~50% when the emulsion temperature increases from 20 to 100 °C. Thus, proper application of the phosphor coating to a heat sink was done to minimize temperature rise caused by plasma exposure under high plasma flux conditions. A range of persistence time values $\tau_p = 1-10\,\mu$s is obtainable depending on the Zn doping level and emulsion grain size. The persistence time of the ZnO:Zn emulsion used in these experiments was measured using a pulsed ultraviolet (UV) (370 nm) source and found to have a $1/e$ decay time of 8 μs. The active particle size in the phosphor emulsion is about 8–15 μm (average density of active sites $\sim 10^8\ \mathrm{cm}^{-2}$) resulting in high spatial resolution.

The response of the ZnO:Zn phosphor to plasma electrons depends on the electron current flux flowing to the disk and the electron impact energy. The response equation can be written as

$$S(\mathbf{r},t) = e \int R(E_e)(\mathbf{v}\cdot\hat{\mathbf{n}}) f_e(\mathbf{r},\mathbf{v},t)\, d^3v, \tag{1}$$

where S is the luminance[6] ($\mathrm{cd/m^2}$), $R(E_e) = S_0 E_e^{1.75}$ is the phosphor response function, $S_0 = 6.94\times 10^{-2}$ cd $(\mathrm{eV})^{-7/4}\,\mathrm{A}^{-1}$, E_e is the electron kinetic energy (eV), f_e is the electron velocity distribution function ($\mathrm{s^3\,m^{-6}}$), and $\hat{\mathbf{n}}$ is the unit normal to the phosphor surface. The previous formula for $R(E_e)$ was obtained by fitting experimental data[7] for ZnO:Zn and is valid for $3.0 \leqslant E_e \leqslant 50$ eV. In the case of ZnO:Zn phosphor the threshold electron energy for phosphor excitation is $E_{ec} \geqslant 3.0$ eV, electrons of lower energy are not detected. In order to detect the plasma electrons it is required that $E_{ec} \ll T_e$, where $T_e \sim 15$ eV in the PISCES–A plasmas. Evaluation of the luminance Eq. (1) using a sheath modified electron Maxwellian velocity distribution function gives the phosphor light intensity dependence on the local electron density n_e, electron temperature T_e, and the disk potential Φ as

$$S(\mathbf{r},t) \cong S_0 \Gamma(15/4)\, \frac{e n_e(\mathbf{r},t)}{\sqrt{2\pi m_e}} (kT_e)^{2.25} \exp[e\Phi(t)/kT_e], \tag{2}$$

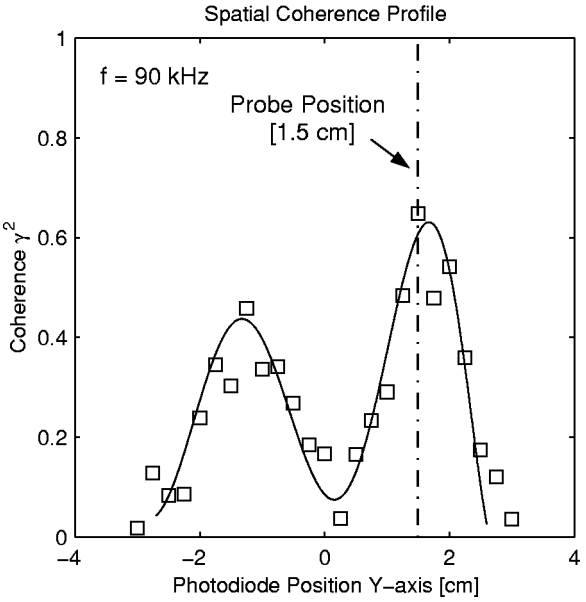

FIG. 3. Density fluctuations caused by a coherent mode in the PISCES–A plasma at $f = 90$ kHz are detected by the photodiode detector focused on the phosphor screen and the Langmuir probe. The spatial coherence between the two measurements indicates the plasma imaging diagnostic is accurately responding to the density fluctuations. The symmetrically positioned high coherence peaks on opposite sides of the plasma axis reveal the spatial structure of the coherent plasma mode.

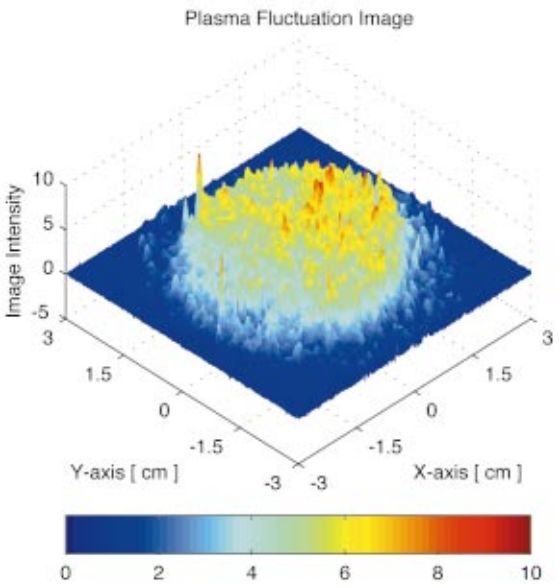

FIG. 4. (Color) A CCD camera image of the plasma excited CAPPIS diagnostic taken with a 1 μs exposure time. The image is plotted as a false color three-dimensional plot and the amplitude distribution and spatial structure of the plasma cross section are evident. The structure in the image has been determined to be statistically significant with SNR$\geqslant$25. The component of the image generated by UV background light has been subtracted. [$B=1000$ G, $P(H_2)=2.5$ mTorr, $kT_e=15$ eV.]

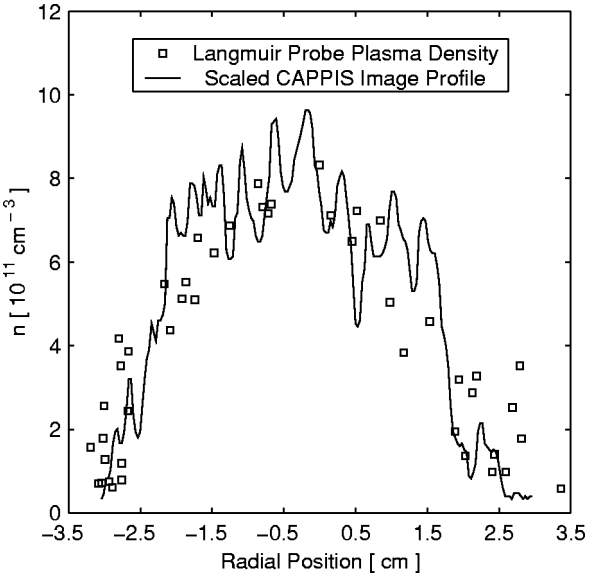

FIG. 5. The spatial profile of the CAPPIS signal and that of a Langmuir probe measurement of the plasma density.

where Φ accounts for the applied bias voltage on the disk and the floating potential. For small amplitude fluctuations Eq. (2) can be expanded to first order as

$$\frac{\tilde{S}}{S}=\frac{\tilde{n}_e}{n_e}+\left(\frac{9}{4}-\frac{e\Phi}{kT_e}\right)\frac{\tilde{T}_e}{T_e}+\frac{e\tilde{\Phi}}{kT_e}, \tag{3}$$

where $\tilde{n}_e$, $\tilde{T}_e$, and $\tilde{\Phi}$ indicate fluctuations in the plasma density, electron temperature, and disk potential, respectively. These equations allow us to interpret 2D phosphor images in terms of the local plasma properties.

We also investigated a ZnS phosphor coating as a candidate for the CAPPIS diagnostic. Plasma imaging with ZnS was unsuccessful and we attributed this to electric charge buildup on the phosphor screen caused by the relatively high surface resistivity of the ZnS layer, $\eta\sim10^{11}\,\Omega$ cm. The other contributing factor was the relatively high threshold energy,[8] $E_{ec}\sim100$ eV of ZnS, making detection of low energy electrons difficult. In contrast, the ZnO:Zn phosphor has a low surface resistivity, $\eta\sim10^{-3}\,\Omega$ cm, which allows an effective electrical bias voltage to be applied to the disk.[9] The brightness of the image can be increased by application of a positive bias voltage $\sim$10 V to the phosphor thus entering the electron collection region of the Langmuir current–voltage characteristic. In the following we discuss results from plasma imaging using an unbiased ZnO:Zn phosphor disk.

IV. EXPERIMENTAL RESULTS

In the following, we report the results of experiments to validate the performance of the CAPPIS diagnostic. The time series data of cathodoluminescent phosphor light is compared with Langmuir probe data and the correlation between light fluctuations and Langmuir probe ion saturation currents is measured. The plasma density profile obtained from Langmuir probe measurements is compared to the CAPPIS image.

The correlation between the CAPPIS light signal and a Langmuir probe is a strong indication that the diagnostic is responding properly to the plasma flux, as predicted by Eq. (1). To measure this correlation, we inserted the phosphor disk into the plasma and monitored the fluctuating light output from a small 0.04 cm^2 region with a 10 MHz bandwidth photodiode and lens setup. The fluctuating phosphor light signal was then compared with local Langmuir probe measurements of the fluctuating plasma ion saturation current. Precise spatial positioning of the focus of the photodetector and lens on the plasma flux tube intercepted by the Langmuir probe results in strongly correlated signals, Fig. 2. The coherence function $0\leqslant\gamma^2\leqslant1$ is defined as $|P_{ij}(\omega)|^2/P_{ii}(\omega)P_{jj}(\omega)$ where $P_{ij}(\omega)$ is the cross-spectral density of the time series signals.[10] A progressive decorrelation of the photosignal and the Langmuir probe signal is found when the photodiode is moved away from the plasma flux tube intercepted by the tip of the Langmuir probe. The spatially dependent coherence profile depicted in Fig. 3 shows how the coherence changes with position when the photodiode is moved to different radial points along the y axis. The coherence profile at $f=90$ kHz in Fig. 3 indicates that the coherence is largest when the probe tip and photodiode focus are on the same magnetic flux tube. The data clearly indicate that the CAPPIS diagnostic is responding to local plasma density fluctuations, further, the coherence profile in Fig. 3 reveals the radial structure of a coherent global plasma mode having a null on axis and a radial wavelength comparable to the plasma radius.

Having established that the CAPPIS diagnostic has the desired local time response to plasma density fluctuations, we can proceed to plasma imaging experiments. An intensified CCD camera was used to obtain microsecond range exposures from the CAPPIS detector. In order to establish the

statistical significance of the image fluctuations it was necessary to perform absolute calibration of the imaging system using a uniform light source. The signal to noise ratio SNR ~ 25 was determined using $\mathrm{SNR} = \sqrt{Q n_p F_M}$, where Q is the photocathode quantum efficiency (8%), n_p is the average number of incident photons ($\sim 10^4$ photons/pixel for 1 μs), and F_M the fill factor of the multichannel plate (~ 0.8).[11] The SNR can be increased with spatial averaging over adjacent pixels. Calibration images were analyzed to study the effect of exposure time, intensifier gain, and light intensity on the response and resolution of the imaging system. The systematic variations in pixel response were removed by use of a correction mask.

The CAPPIS image is actually a composite of two effects, electron impact excitation of the phosphor and a background of UV photon excitation caused by atomic line radiation from the plasma, e.g., Lyman series in hydrogenic plasmas. In order to remove the UV background contribution we subtract a smooth profile from a fitted model of the UV illumination.

An example of a 1 μs exposure CAPPIS image of the PISCES plasma cross section is shown in Fig. 4. The image in Fig. 4 has been spatially filtered to a resolution of 1 mm^2. Analysis of the intensity fluctuations in Fig. 4 for $r < 3$ cm (inside the plasma column) indicates $\tilde{S}/S \sim 30\%$. Overall, we find that spatial plasma density fluctuations of amplitude $\tilde{n}/n > 5\%$ can be detected with the present setup. In Fig. 5 we compare plasma density profiles obtained from a vertical Langmuir probe scan and a vertical intensity chord from the image in Fig. 4. The two profiles in Fig. 5 are in good agreement and demonstrate the high spatial resolution contained in a CAPPIS image.

[1] S. Zweben and R. Gould, Nucl. Fusion **25**, 171 (1985).
[2] A. Chakhovskoi, W. Kesling, J. Trujillo, and C. Hunt, J. Vac. Sci. Technol. B **12**, 785 (1994).
[3] J. Kamler, *Luminescent Screens, Photometry and Colorimetry* (1969).
[4] L. Shea, *The Electrochemical Society Interface* (1998).
[5] Z. Lin, R. Boivin, and S. Zweben, PPPL-TM-392 (1992).
[6] C. DeCusatis, *Handbook of Applied Photometry* (AIP, Woodbury, NY, 1997).
[7] K. Narita, A. Kagami, and Y. Mimura, J. Electrochem. Soc. **127**, 1794 (1980).
[8] M. Anderson, M. Phillips, and R. Walko, J. Mater. Res. Soc. **348**, 497 (1994).
[9] Y. Li, E. Forsythe, G. Tompa, J. Liu, and D. Morton, Mater. Res. Soc. Symp. Proc. **441**, 615 (1997).
[10] J. Bendat and A. Piersol, *Random Data, Analysis and Measurement Procedures* (1986).
[11] E. Dereniak and D. Crowe, *Optical Radiation Detectors* (1984).